# Coastline Direction, Interannual Flow, and the Strong El Niño Currents along Australia's Nearly Zonal Southern Coast

JIANKE LI AND ALLAN J. CLARKE

*Oceanography Department, The Florida State University, Tallahassee, Florida*

(Manuscript received 13 January 2004, in final form 26 May 2004)

ABSTRACT

The western equatorial Pacific Ocean El Niño signal leaks through the gappy western equatorial Pacific Ocean boundary to the western and southern coasts of Australia. Ocean Topography Experiment (TOPEX)/Poseidon sea level data and coastal tide gauge measurements show that off the northwest coast the low-frequency signal propagates westward as large-scale Rossby waves. However, along the nearly zonal southern coast, particle displacements are nearly zonal near the coast and experience no planetary vorticity change. As a consequence, the Rossby wave mechanism fails, and theory suggests that the signal should decay from the shelf edge with baroclinic Rossby radius-of-deformation scale. High-resolution along-track TOPEX/Poseidon sea level heights show that the interannual height signal does decay rapidly seaward of the shelf edge with this scale. The sharp fall in sea level and geostrophic balance imply strong ($\sim$10 cm s$^{-1}$) low-frequency currents seaward of the shelf edge. On the shelf, interannual flow is in the same direction as the shelf-edge flow but is much weaker. The anomalous flows tend to be eastward during La Niña, when the western equatorial Pacific and Australian coastal sea levels are unusually high, and westward during El Niño when coastal sea levels tend to be anomalously low. The anomalous low-frequency flows can transport larvae large distances, enhancing the recruitment of Australian salmon to nursery grounds in the eastern part of the southern coast when the coastal sea level is higher than normal and decreasing recruitment when it is lower than normal.

## 1. Introduction

During an El Niño, anomalous westerly equatorial winds push equatorial water eastward, lowering sea level in the western equatorial Pacific Ocean. Because of gaps in the western equatorial Pacific boundary, sea level is lowered around western New Guinea. Consistent with geostrophic balance and no normal flow into the coast at interannual frequencies, the sea level should be spatially constant and lower all along the west coasts of New Guinea and western and southern Australia (Fig. 1). During La Niña, the equatorial winds are anomalously easterly and the sea level should be anomalously high in the western equatorial Pacific and the western and southern coasts of Australia. Pariwono et al. (1986) first discovered that there was an Australian interannual coastal sea level signal and that it was correlated with El Niño. Clarke (1991) suggested that this was due to the leaky western equatorial Pacific mechanism discussed above.

Australia's western and southern coastlines vary considerably in direction. While much of the western coastline is nearly meridional, Australia's southern coastline is unusual in that part of it is nearly zonal for over 1000 km. Theoretically the angle of the coastline to due north should fundamentally affect the interannual coastal flow (Schopf et al. 1981; Clarke 1983, 1992; Grimshaw and Allen 1988; Clarke and Shi 1991). Specifically, at low enough frequency, along an eastern ocean boundary that is not nearly zonal, low-frequency coastal energy propagates westward into the interior ocean as long Rossby waves. Along a nearly zonal coastline like that off part of southern Australia, however, particles of fluid do not experience a change in Coriolis parameter because the flow is parallel to the coast and therefore east–west. Consequently, the Rossby wave mechanism does not operate and $f$-plane dynamics applies. When $f$-plane dynamics applies and, as in this case, the ocean is not locally forced by the wind, the flow should behave like a coastal Kelvin wave (see, e.g., Clarke 1983). Since we expect the deep-sea signal leaked through the western equatorial Pacific boundary to be mainly in the first two vertical modes (Clarke and Liu 1994), in accordance with Kelvin wave dynamics the deep-sea El Niño signal should decay away from the southern boundary with first and second baroclinic radius-of-deformation scales. Because the first baroclinic radius-of-deformation scale is larger, we expect the ENSO signal to be trapped within approximately a first baroclinic radius of deformation of the boundary. The sharp decay of sea level away from the boundary means, by geostrophy, that strong

*Corresponding author address:* Allan J. Clarke, Oceanography Department, The Florida State University, Tallahassee, FL 32306-4320. E-mail: clarke@ocean.fsu.edu

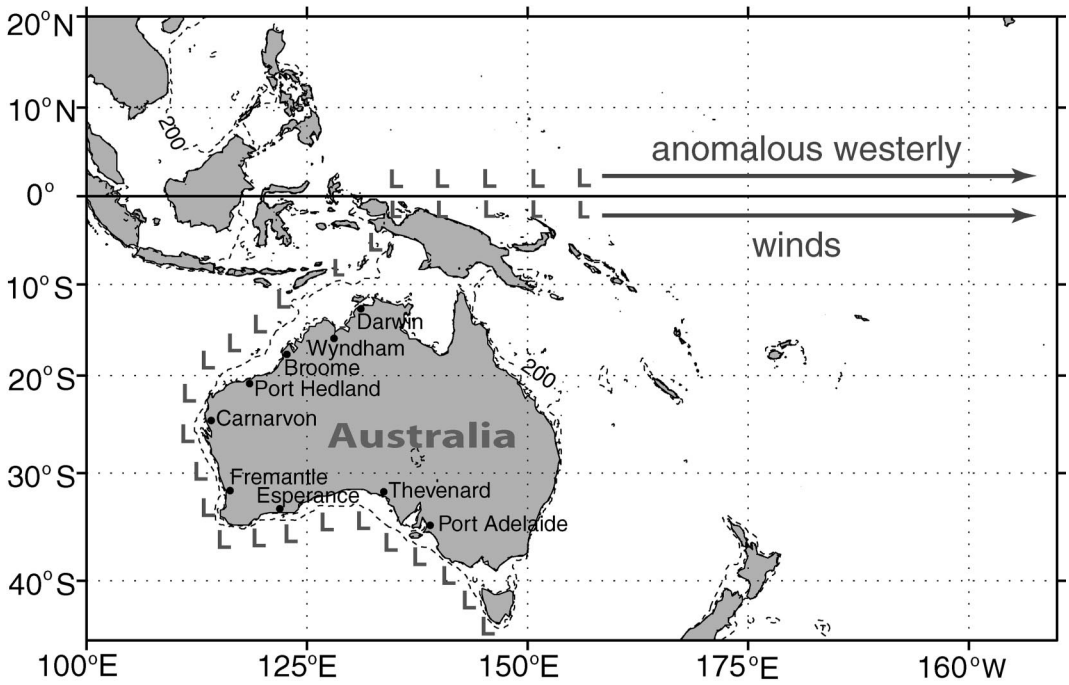


FIG. 1. Western equatorial Pacific showing the 200-m isobath (dashed line) around Australia and the anomalous low sea level (L) resulting from the anomalous equatorial westerly winds, which blow in the central equatorial Pacific between about 160°E and 150°W during El Niño. Anomalous equatorial easterly winds blow during La Niña, and the sea level around western and southern Australia tends to be higher than normal.

alongshore flows should be present. Such very low frequency flows can move larvae long distances and fundamentally affect coastal marine populations.

The southern Australian coast is a good place to test whether coastline angle makes a difference to low-frequency flow because, as noted above, there is an interannual coastal sea level signal extending along a coastline that is nearly zonal over thousands of kilometers. To be more precise about whether Rossby or Kelvin wave dynamics applies, consider a constant-depth ocean with flow of frequency $\omega$ near a boundary making an angle $\theta$ with due north (Fig. 2). If the motion is all in a given vertical mode with gravity wave speed $c$, then motion is trapped near the boundary if (see, e.g., Clarke and Shi 1991)

$$\omega > \beta c \cos\theta/(2|f|), \tag{1.1}$$

where $\beta$ is the northward gradient of the Coriolis parameter $f$. For interannual sea level and the first vertical mode along Australia's southern coast, $|f| = 8 \times 10^{-5}$ s$^{-1}$, $c = 2.7$ m s$^{-1}$, $\beta = 2 \times 10^{-11}$ m$^{-1}$ s$^{-1}$, and $\omega = 2\pi/3$ yr. It follows from (1.1) that for trapping, $|90° - \theta| < 11°$; that is, the coastline angle has to be within about 11° of due east. For the second and higher vertical modes, $c$ is smaller and the coastline direction does not have to be as zonal for trapping. Thus all baroclinic modes should be trapped for coastline angles within about 11° of due east. This condition is satisfied for hundreds of kilometers along Australia's southern continental shelf edge where the deep sea begins and the vertical-mode theory is approximately applicable.

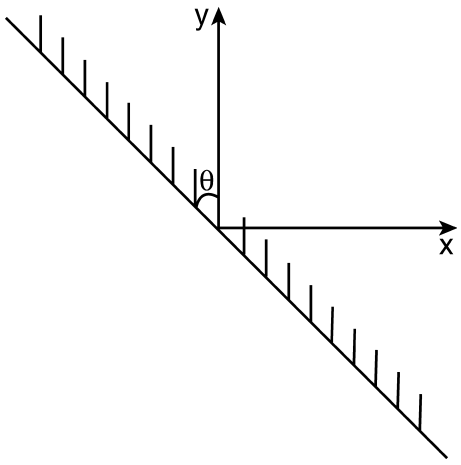


FIG. 2. Definition of $\theta$, the angle that the coastline makes with due north. Note that, when $90° < \theta < 270°$, the coastal boundary becomes a ''western'' ocean boundary.

In the next section we describe and discuss the observed interannual sea level along Australia's western and southern coasts using more accurate coastal data than those available to Pariwono et al. (1986). In addition, Ocean Topography Experiment (TOPEX)/Poseidon satellite sea level height estimates are now nearly a decade long and enable us to examine interannual sea

TABLE 1. The coastal sea level stations.

| Stations | Lat (S) | Lon (E) |
|---|---|---|
| Darwin | 12°28′ | 130°51′ |
| Wyndham | 15°27′ | 128°06′ |
| Broome | 18°00′ | 122°13′ |
| Port Hedland | 20°19′ | 118°34′ |
| Carnarvon | 24°54′ | 113°39′ |
| Fremantle | 32°03′ | 115°43′ |
| Esperance | 33°52′ | 121°54′ |
| Thevenard | 32°09′ | 133°39′ |
| Port Adelaide | 34°51′ | 138°30′ |

level behavior off the western and southern Australian coasts. Together with the coastal data they enable us to test the ideas mentioned earlier about the effect of coastline direction on the interannual sea level (section 3) and also enable us to calculate the strength and structure of the interannual flows (section 4). Interannual currents can affect the transportation of larvae and hence marine populations. In section 5 we discuss the effect of the interannual current on the distribution of western Australian salmon. Section 6 contains concluding remarks.

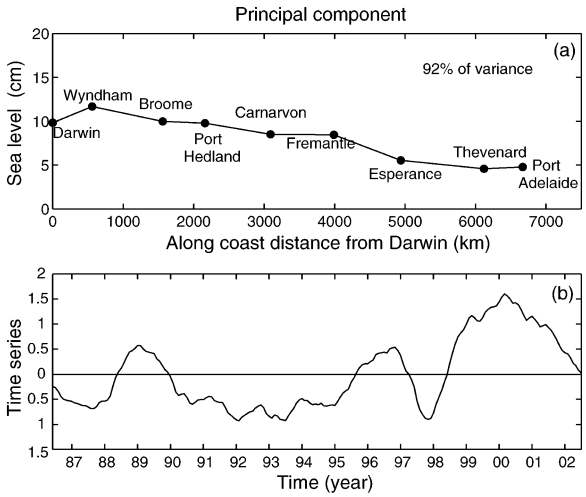


FIG. 3. (a) Alongshore structure of the first empirical orthogonal function of interannual sea level (cm) for the nine coastal stations shown in Table 1. This EOF explains 92% of the variance. The original monthly time series, with seasonal cycle removed and corrected for atmosphere pressure, were filtered interannually using the filter of Trenberth (1984). (b) The principal component time series corresponding to the EOF in (a). The time series is normalized with variance 0.5.

## 2. Observed coastal interannual sea level

We base our analysis of coastal interannual sea level on monthly sea level data obtained from Australia's National Tidal Facility and monthly atmospheric pressure data provided by the National Oceanic and Atmospheric Administration (NOAA)–Cooperative Institute for Research in Environmental Sciences (CIRES) Climate Diagnostics Center in Boulder, Colorado, from their Web site online at http://www.cdc.noaa.gov/. The coastal sea level records were available for nine stations (see Fig. 1 and Table 1) from January 1986 to December 2002. We adjusted these data for atmosphere pressure to obtain monthly adjusted sea level corresponding to the near-surface ocean pressure relevant to ocean dynamics. After removing the seasonal cycle of the monthly adjusted sea level, we filtered the resulting anomalies with an 11-point centered filter (Trenberth 1984) to obtain the interannual signal. The unadjusted and adjusted interannual sea level signals were almost identical.

An empirical orthogonal function (EOF) analysis of the nine coastal interannual sea level time series showed that 92% of the variance could be explained by the first EOF mode (Fig. 3). We normalized the principal-component time series to have a variance of 0.5 so that the EOF structure function (Fig. 3a) is representative of sea level amplitude. The dominance of a single EOF over more than 6000 km of coastline shows that the sea level is in phase all along the coast. This in-phase relationship is confirmed by a lagged regression analysis of the nine sea level stations, which showed that the maximum correlation between stations was at zero lag. At first sight this zero lag result seems to contradict theory because, as mentioned earlier, along Australia's nearly zonal southern coast Kelvin wave dynamics should apply and a phase lag should result from Kelvin wave propagation. However, the lag cannot be resolved by our monthly data because at a speed of 2.7 m $s^{-1}$, it takes less than a week for the Kelvin wave to travel along the zonal part of the shelf edge.

The principal-component time series of the EOF is highly correlated ($r = -0.80$) with the El Niño index Niño-3.4 [the average equatorial Pacific sea surface temperature anomaly in the region (5°N–5°S, 170°–120°W)], but the record is short on an interannual time scale. However, the correlation was confirmed using the 50-yr interannual record at Fremantle ($r = -0.71$) and is also consistent with the plots in Pariwono et al. (1986).

The in-phase and correlation results are in agreement with the equatorial western Pacific leak mechanism discussed in the introduction, but the alongshore structure of the signal is not; the EOF in Fig. 3a shows that the coastal amplitude is not constant, as one would expect, but rather decreases along the coast from about 10 cm on Australia's northwest coast to about 5 cm on Australia's southern coast. This fall in signal amplitude was confirmed by the lagged regression analysis of the nine sea level stations and also a lagged regression calculation of interannual sea level for Fremantle, Thevenard, and Port Adelaide over a much longer record from 1934 to 2002.

The decrease in interannual coastal sea level amplitude along the coast is inconsistent with geostrophic balance at a frictionless vertical coastal wall. But in the real world, the flow is not frictionless and the bottom topography is not vertical. Bottom friction can dissipate the interannual signal (Clarke and Van Gorder 1994)

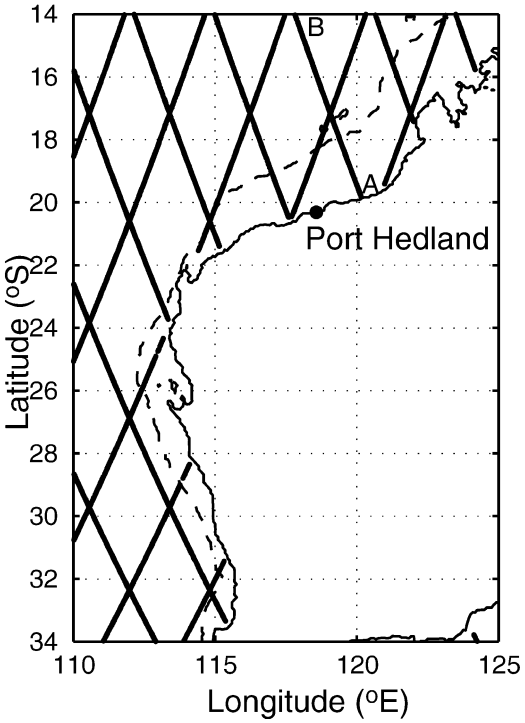


FIG. 4. TOPEX/Poseidon tracks near the western Australian coast. Sea level heights along track AB are analyzed in Fig. 5. The dashed line, marking the 200-m isobath, shows the approximate position of the shelf edge.

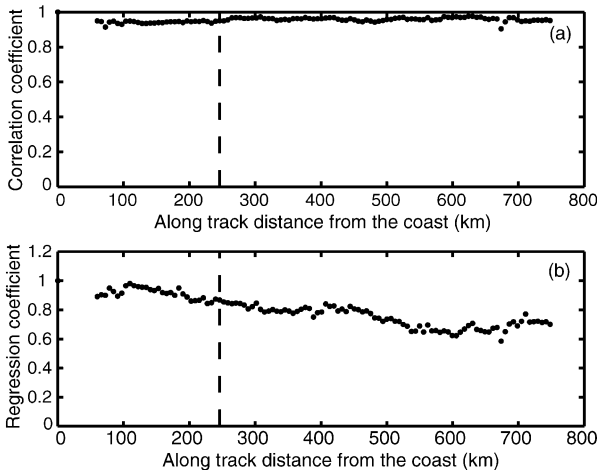


FIG. 5. (a) Correlation of the interannual sea level estimates along track AB shown in Fig. 4 with the nearest interannual coastal tide gauge time series at Port Hedland. The correlations begin about 50 km from the coast, and the dashed line denotes the approximate position of the shelf edge. (b) Regression coefficients corresponding to (a).

although it only seems to be active close to the coast where the water is well mixed (Pizarro et al. 2001) because farther from the coast bottom boundary layer transport along a sloping bottom topography under a stratified fluid can stop frictional drag (MacCready and Rhines 1993; Trowbridge and Lentz 1991). The fall in amplitude of the interannual signal may also be caused by the large-scale flow losing energy to eddies that are prevalent along the coast (see, e.g., Tomczak and Godfrey 1994).

## 3. Offshore interannual sea level

As mentioned in the introduction, in theory coastline direction should strongly influence the dynamics of the near-coast interannual flow. We will test this using offshore TOPEX/Poseidon satellite sea level height estimates. The TOPEX/Poseidon satellite measures sea level at about every 6–7 km, repeating the measurement every 10 days along tracks about 250–300 km apart. The along-track estimates are usually spatially averaged to reduce the noise, but at a cost of decreased spatial resolution. Here we need high spatial resolution to accurately estimate the sea level gradient and associated geostrophic flow. Since we are interested in low-frequency flow we can remove noise by averaging in time, first forming monthly TOPEX/Poseidon sea level heights from the 10-day estimates and then filtering using the same interannual filter (Trenberth 1984) as for the coastal time series. Although the raw monthly satellite records are nearly a decade long, beginning in January 1993 and ending in April 2002, they are still short on an interannual time scale. Therefore, our results, while suggestive and consistent with theory, await confirmation by longer records.

### *a. Sea level off the western Australian coast*

Figure 4 shows TOPEX/Poseidon tracks off Australia's western coast, and Fig. 5 is a plot of correlation and regression coefficients of satellite-estimated interannual sea level along track AB with interannual tide gauge sea level at Port Hedland. Raw satellite sea level height estimates are subject to increased error near the coast, and points closer to the coast than about 50 km were not used. If the offshore and coastal interannual signals were the same, then the correlation and regression coefficients would both be unity; correlation and regression coefficients both decrease if the offshore and coastal signals differ due to measurement error and/or westward propagation in the offshore signal. As found by Clarke and Li (2004), the correlation coefficient is nearly 1 for all points along the track and the regression coefficient decreases only very slowly from unity from the coast. These results are consistent with the expected large-scale westward Rossby wave propagation and the sea level hardly changing along the coast.

We checked the theory further by testing for westward Rossby wave propagation. Since the spatial scales are large at low latitudes, we could afford to use the lower-resolution $1^\circ \times 1^\circ$ data, filtered in the same way as before to get interannual gridpoint time series. We lag correlated the monthly gridpoint time series with the monthly coast-

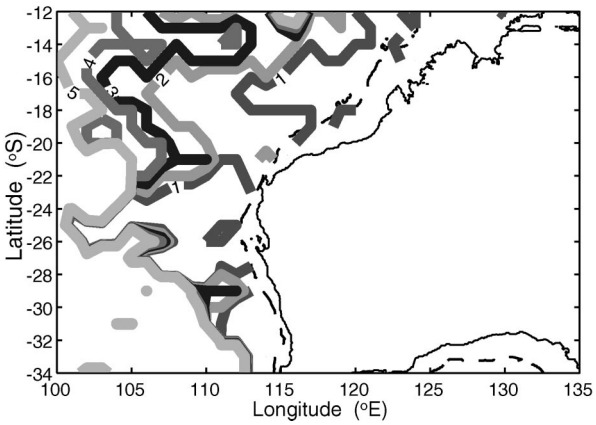


FIG. 6. The lag (months) at maximum correlation between satellite estimates of interannual sea level and the coastal sea level time series. A positive lag corresponds to westward propagation. Lags greater than 5 months are not plotted. The dashed line is the 200-m isobath.

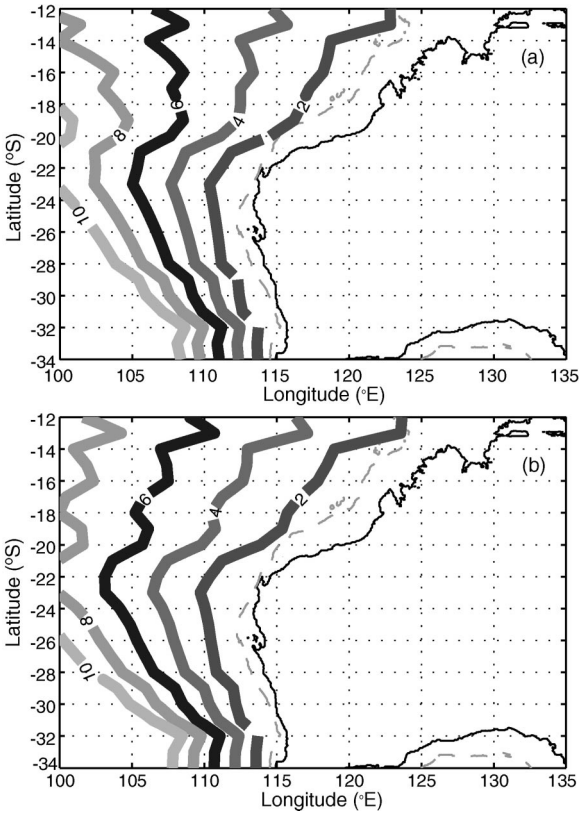


FIG. 7. Theoretical lag (months) for long westward-propagating, first-vertical-mode Rossby waves when (a) $\overline{u} = 0$ and (b) $\overline{u} \neq 0$. Lags greater than 10 months are not plotted.

al sea level time series found from the first EOF of the coastal sea level records off the western Australian coast. At each grid point we recorded the lag at maximum correlation and have plotted the results in Fig. 6. The increasing lag westward off the northwest Australian coast implies westward propagation, which is faster nearer the equator. The latter is in qualitative agreement with the long-wave Rossby wave speed $\beta c^2/f^2$ since this is larger nearer the equator. South of about 23°S the lags are noisier and the correlations are lower.

To check the observed lags with theory quantitatively, we used the theory of Killworth et al. (1997), which takes into account mean zonal ocean flow. Assuming a 1000-m depth level of no motion, we calculated the mean flow using the Levitus *World Ocean Atlas 1994* data provided by the NOAA–CIRES Climate Diagnostics Center. These data are available online at the Web site http://www.cdc.noaa.gov. The mean eastward flow south of about 22°S is typically about 4 cm $s^{-1}$ near the surface, decreasing to zero at 300-m depth. The theoretically estimated monthly interannual sea level assumed that the given coastal sea level was all in vertical mode 1.

Off northwestern Australia, observations (Fig. 6) and theory with or without zonal mean flow (Figs. 7a,b) agree qualitatively in that the spatial scales are large, that there is westward propagation, and that it is faster nearer the equator; quantitatively the observed speeds are too fast. This may be because the record is too short to accurately estimate the lags. The strong mean zonal onshore flow south of about 23°S does not affect the lags very much (cf. Fig. 7a and Fig. 7b), and so it is probably not the explanation for the observed noisy lags and low correlations. Another possibility is that the Rossby wave signal is distorted by the Leeuwin Current, a strong (~50 cm $s^{-1}$) 70-km-wide current running parallel to and seaward of the shelf edge. Clarke and Li (2004) showed that in the region of the Leeuwin Current the Rossby wave dynamical balance no longer applies. They showed theoretically and observationally that the ENSO signal decays rapidly from the shelf edge with a scale on the order of the width of the Leeuwin Current. The ENSO signal seaward of the Leeuwin Current is weak and may not be able to be seen above eddy and other noise.

### *b. Sea level off the southern coast*

An EOF analysis of interannual sea level for the three southern coastal stations for the period from January 1993 to April 2002 for which we have satellite data shows that the first mode explains 95% of the variance and, similar to Fig. 3, these stations have similar amplitudes. Therefore we can represent the interannual sea level along the southern coast as an average of the interannual sea level at these three stations.

The correlation and regression coefficients between the along-track TOPEX/Poseidon satellite-estimated interannual sea level signal and the interannual coastal sea level signal show how the sea level changes away from the coast. Because of the large extent of the nearly zonal coastline, we use the data of tracks 6, 12, and 17 in Fig. 8 to represent the ocean signals at the west, middle, and east of the area in which we are interested. Raw satellite

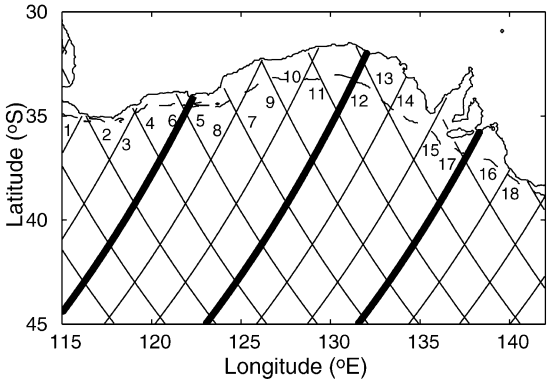


FIG. 8. TOPEX/Poseidon tracks near the southern Australia coast. Sea level heights along tracks 6, 12, and 17 (thick lines) are analyzed in Fig. 9. The dashed line, marking the 200-m isobath, shows the approximate position of the shelf edge.

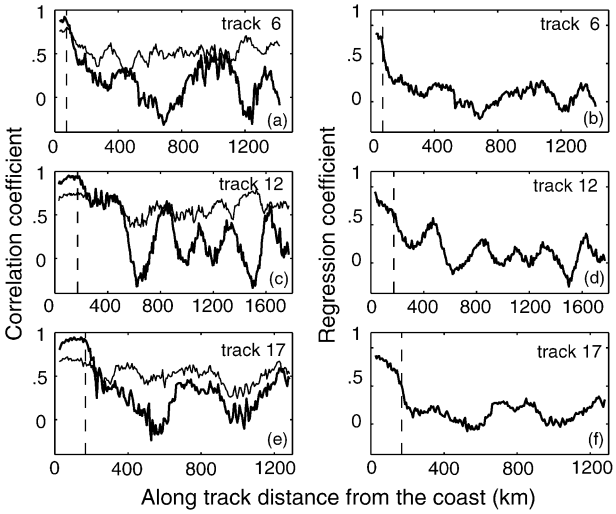


FIG. 9. (a) Correlation of the interannual sea level estimates along track 6 shown in Fig. 8 with the interannual coastal sea level time series (average of interannual coastal sea level at Esperance, Thevenard, and Port Adelaide). The correlations begin about 30 km from the coast, and the dashed line denotes the approximate position of the shelf edge. The 95% critical correlation coefficients marked by the thin lines were found using the method of Ebisuzaki (1997). (b) Regression coefficients corresponding to (a). (c) and (d) As in (a) and (b) but for track 12; (e) and (f) for track 17.

sea level height estimates are subject to increased error near the coast, and points closer to the coast than about 30 km along track were not used. In all three tracks both the correlation coefficient and the regression coefficient drop suddenly away from the shelf edge (Fig. 9).

To understand this behavior, suppose that the coastal interannual sea level is a pure large-scale signal $s(t)$ and the satellite interannual sea level estimate at a given location is $\alpha s(t) + \varepsilon(t)$, where $\alpha$ is a constant and $\varepsilon(t)$ is uncorrelated ''noise.'' That the coastal sea level is a pure signal is reasonable given the similarity of the three widely separated coastal sea level stations. The noise $\varepsilon(t)$ is most likely due to eddies. In the absence of noise the regression coefficient is $\alpha$ and the correlation coefficient is unity. The observed sharp fall in the regression and correlation coefficients seaward of the shelf edge is consistent with either a sharp fall in offshore sea level signal ($\alpha < 1$) and small to moderate amplitude noise or with an essentially unchanged offshore signal ($\alpha \approx 1$) and noise of larger amplitude than the signal. In the latter case the root-mean-squared (rms) sea level would increase offshore. However, calculations show that the rms sea level decreases, consistent with a fall in the amplitude of the coastal signal.

A decreased signal seaward of the shelf edge is consistent with Kelvin wave dynamics. As noted earlier, we expect that this baroclinic signal will decay seaward with the first baroclinic radius of deformation scale. At 35°S, the expected decay scale is $c/|f| \approx 32$ km for $c = 2.7$ m s$^{-1}$, and this is similar to the scale of the sharp drop in the regression coefficient near the shelf edge for tracks 6, 12, and 17.

## 4. Interannual currents

### *a. The current along the shelf edge*

By geostrophy, the sharp fall in interannual sea level just seaward of the shelf edge must correspond to a strong interannual current there. The sea level data along a single track give us only the component perpendicular to the track. However, at some points near the shelf edge, where satellite tracks cross and thus give us two velocity components at a given point, flow direction and magnitude near the shelf edge can be checked. The amplitudes of the velocity at the intersecting points A, B, and C in Fig. 10 are about 4.4, 1.5, and 1.6 cm s$^{-1}$, respectively, and the current directions are almost parallel to the local shelf edge, as we would expect.

Assuming that all flows near the shelf edge are parallel to the shelf edge, we can estimate the speed of the flow along the shelf edge at several other points. All

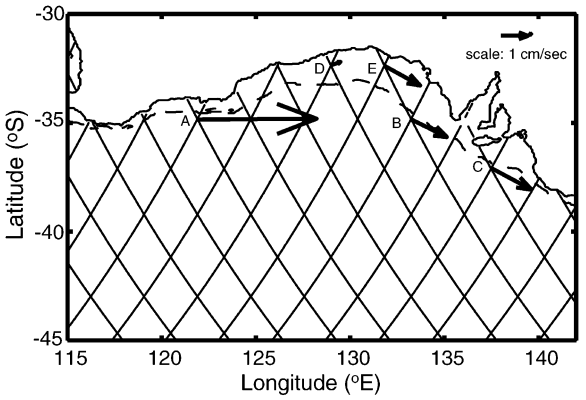


FIG. 10. The along-shelf-edge current at the two-track intersection points A, B, and C and the shelf current at points D and E. The directions of the current are almost parallel to the local isobath.

TABLE 2. The along-shelf-edge current at points along the southern Australian coast where the satellite tracks cross the shelf edge (see Fig. 8). The reported longitude is where the TOPEX/Poseidon satellite track crosses the shelf edge.

| Lon (°E) | 116.0 | 116.5 | 118.9 | 119.1 | 121.7 | 122.1 | 124.4 | 125.3 | 126.6 |
|---|---|---|---|---|---|---|---|---|---|
| Track | 1 | 2 | 3 | 4 | 5 | 6 | 7 | 8 | 9 |
| Speed (cm $s^{-1}$) | 10.9 | 10.2 | 7.6 | 6.4 | 8.7 | 8.9 | 7.1 | 7.0 | 7.2 |
| Lon (°E) | 128.5 | 129.5 | 131.3 | 132.9 | 133.4 | 135.5 | 137.2 | 137.6 | 139.9 |
| Track | 10 | 11 | 12 | 13 | 14 | 15 | 16 | 17 | 18 |
| Speed (cm $s^{-1}$) | 7.2 | 6.1 | 4.3 | 3.5 | 2.8 | 1.1 | 3.9 | 3.5 | 1.1 |

we need is one track that crosses the shelf edge and the angle between the track and the shelf edge. The results of such shelf-edge velocity calculations are shown in Table 2. Along-shelf-edge currents are larger in the west (tracks 1–11) than in the east (tracks 12–18). Consequently sea level gradients are stronger in the west where much of the shelf edge (tracks 1, 2, 5, 6, 9–11) is nearly zonal. Tracks 3, 4, 7, and 8 in the west do intersect a nonzonal shelf edge and yet still have strong sea level gradients. However, the shelf edge is a western boundary type in that the ocean is to the *east* of the land ($90° < \theta < 270°$ in Fig. 2). Rossby wave energy leaving such a boundary must have eastward group velocity, small wavelengths, and much larger sea level gradients than at an eastern boundary [see, e.g., the low-frequency near-boundary solution, Eq. (A6) in Clarke (1983)]. In practice we do not expect the high-wavenumber linear Rossby wave solution to be quantitatively accurate, but we do expect shorter spatial sea level scales at the western boundary type of coast (tracks 3, 4, 7, and 8) than in the east (tracks 12–18).

Cirano and Middleton (2004) commented on some in situ shelf-edge current measurements off southeastern Australia (35°46′S, 135°45′E and 37°32′S, 139°31′E) that are consistent with the satellite-derived geostrophic flow. Although the records are ''short'' (97 days in the first location and 57 and 59 days in the second), they occurred at the height of the El Niño in 1982 and after the El Niño in 1983. As expected, the shelf-edge currents increased markedly eastward from the conditions during the anomalously low coastal sea level El Niño in 1982 to the post–El Niño conditions of 1983.

### *b. Average interannual shelf current*

An examination of Fig. 9 shows that on wide shelves the regression coefficients not only drop away from the shelf edge but also, with smaller slope, decay away from the coast. Theoretically, low-frequency, linear, $f$-plane flow of constant-density water over the continental shelf should approximately follow the isobaths. We can see this at points D and E of Fig. 10 where two tracks intersect and we can calculate the vector velocity. Assuming that flow follows the isobaths, we can estimate the average shelf velocities from a single track just as we estimated the shelf-edge velocities (Table 3). These along-shelf currents are in the same direction as the shelf-edge flow but are much weaker ($\sim$2 cm $s^{-1}$ as compared with as much as 10 cm $s^{-1}$).

## 5. The effect of interannual flow on the distribution of western Australian salmon

Western Australian salmon (*Arripis truttaceus*) looks like a salmon but is really a perch. It spawns off Australia's southwestern coast (Fig. 11) during March and April. While some larvae settle near southwestern Australia, many are transported eastward by the Leeuwin Current and settle about 3–6 months later in protected coastal waters more than 1000 km to the east (see arrows in Fig. 11). The salmon begin their journey being only millimeters in length but grow to 5–8 cm by the time they reach the nursery areas in the east. The juvenile fish spend 6–12 months in these inshore nurseries and then swim to more exposed coasts where they aggregate in large schools seaward of the surf zone. After several years, during which time the salmon can grow to 80 cm in length, the fish migrate back to the western Australian spawning region in November–January and start the life cycle again.

The interannual flow discussed earlier should affect the transport of the salmon larvae from western Australian to south Australian waters and thus the recruitment of first-year salmon into the fishery. For example, if only interannual flow of frequency $\omega$ influenced the transport, the amplitude of the displacement eastward would be the eastward current amplitude/$\omega \sim$ 1200 km using a typical current amplitude of 8 cm $s^{-1}$ (see Table 2) and $\omega = 2\pi/(3\ \text{yr})$. August is usually the month during which salmon enter the nursery areas near Port

TABLE 3. The along-shelf current averaged across the shelf.

| | Track No. | | | | | | | | |
|---|---|---|---|---|---|---|---|---|---|
| | 8 | 9 | 10 | 11 | 12 | 13 | 14 | 15 | 17 |
| Speed (cm $s^{-1}$) | 1.6 | 1.1 | 0.6 | 1.2 | 2.0 | 1.1 | 1.2 | 1.6 | 2.2 |

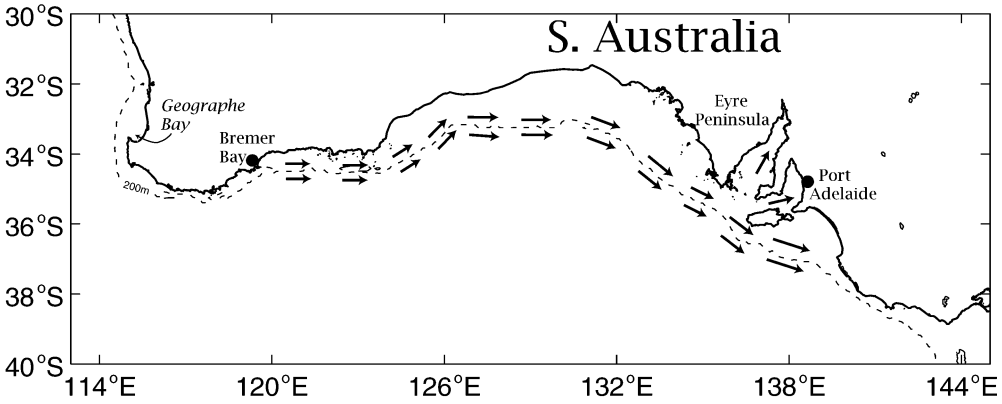


FIG. 11. The southern Australian coast and 200-m isobath. Spawning mainly occurs between Geographe Bay and Bremer Bay during Mar and Apr. Some larvae settle locally, but many eggs and larvae are advected eastward to the protected coastal nursery grounds east of Eyre Peninsula.

Adelaide (see Fig. 1), and Lenanton et al. (1991) showed that, for the period 1979–89, Port Adelaide sea level in August was well correlated ($r = 0.80$) with $\ln(n)$, where $n$ is an estimate of the number of salmon recruits. However, using logarithmic recruitment data generously supplied by K. Jones (2003, personal communication) over the longer period 1981–82 and 1984–99, this correlation falls to $r = 0.53$ with 95% confidence limits $r = 0.08$ and $r = 0.80$. One might argue that, since the salmon eggs and larvae are being affected by flow from about March to September, the recruitment index should be proportional to the flow from March to September. Earlier we showed that the low-frequency flow is proportional to coastal sea level and, because the sea level at Port Adelaide is representative of sea level all along the southern Australian coast (see Fig. 3), the anomalous transport from March to September should be well represented by Port Adelaide sea level from March to September. Figure 12 shows that there is an approximate linear relationship between this flow index and the recruitment index. The correlation coefficient is $r = 0.60$ with 95% confidence limits $r = 0.08$ and $r = 0.80$. This is what we would expect physically: higher coastal sea level corresponds to a stronger eastward flow and more recruits, while lower sea level corresponds to weaker eastward flow and fewer recruits.

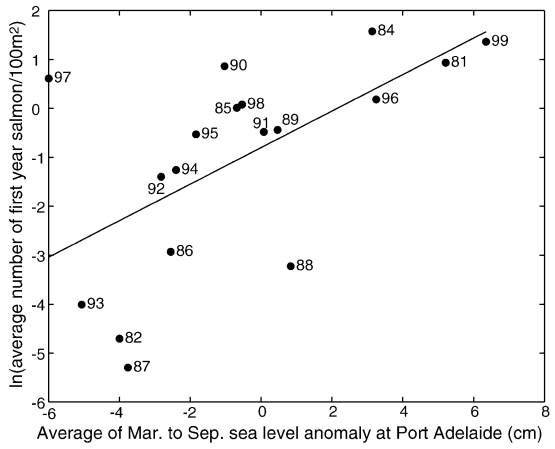


FIG. 12. Relationship between the prerecruit indices (natural logarithm of average number of first-year salmon per 100 square meters) for Australian salmon in south Australian waters, 1981–99 with 1983 missing, and the average of sea level anomaly from Mar to Sep at Port Adelaide in that year.

The recruitment index is logarithmic, and so Fig. 12 suggests that salmon recruitment is exponentially dependent on anomalous sea level. This sensitivity results in an enormous recruitment range (a factor of over 1000). The exponential dependence can be explained using a similar argument to that used by Clarke and Li (2004).

Specifically, when the March–September coastal sea level rises by a small amount $\delta\eta$ then the eastward current will increase by a corresponding proportional amount

$$\delta u = \nu\delta\eta. \tag{5.1}$$

We postulate that the small fractional increase $\delta n/n$ in the number $n$ of salmon recruited is proportional to $\delta u$ so that from (5.1) we may write, for some constant $\lambda$,

$$\delta n/n = \lambda\delta\eta. \tag{5.2}$$

Integrating this equation from no-anomaly conditions when the sea level anomaly $\eta = 0$ and $n = n_0$ to some general anomaly condition $\eta$ and $n$ gives

$$\ln(n/n_0) = \lambda\eta, \tag{5.3}$$

the theoretical counterpart of Fig. 12.

## 6. Conclusions

The El Niño sea level signal leaks through gaps in the western equatorial Pacific and around Australia's western and southern coasts. Australia's coastline varies greatly in direction and, in agreement with theory, TOPEX/Poseidon sea level height estimates, together with coastal sea level data, show that coastline direction fun-

damentally affects the dynamics. Australia's northwest coast is not nearly zonal, and the interannual signal propagates westward with spatial scale comparable to that expected for long, westward-propagating Rossby waves. The southern coast of Australia is nearly zonal, however, and so particle paths near the coast are nearly zonal and experience little change in planetary vorticity. Rossby wave dynamics does not apply, and the interannual signal has properties similar to a coastal Kelvin wave. The signal decays sharply from the shelf edge, with a scale comparable to the baroclinic radius of deformation. By geostrophy, the sharp sea level gradients give rise to anomalous eastward flow when the coastal sea level is higher than normal (typically during La Niña) and anomalous westward flow when the coastal sea level is lower than normal (typically during El Niño). Shelf currents are weaker and in the same direction as the anomalous flow parallel to the shelf edge. The anomalous flow affects the March–September eastward transport of Australian salmon larvae from western Australia by the mean eastward flow, enhancing recruitment in the eastern nursery grounds when the March–September sea level is high and decreasing it when it is low.

*Acknowledgments.* We thank Dr. Keith Jones of the South Australian Research and Development Institute for the salmon data, Australia's National Tidal Facility and the Permanent Service for Mean Sea Level for the coastal sea level data, the National Aeronautics and Space Administration for the TOPEX/Poseidon sea level height estimates, and the NOAA–CIRES Climate Diagnostics Center for the surface pressure data. John Middleton commented helpfully on the manuscript. We also gratefully acknowledge funding from the National Science Foundation (OCE-9818650 and OCE-0220563).

## REFERENCES

Cirano, M., and J. F. Middleton, 2004: Aspects of the mean winter circulation along Australia's southern shelves: Numerical studies. *J. Phys. Oceanogr.,* **34,** 668–684.

Clarke, A. J., 1983: The reflection of equatorial waves from oceanic boundaries. *J. Phys. Oceanogr.,* **13,** 1193–1207.

——, 1991: On the reflection and transmission of low-frequency energy at the irregular western Pacific Ocean boundary. *J. Geophys. Res.,* **96,** 3289–3305.

——, 1992: Low frequency reflection from a nonmeridional eastern ocean boundary and the use of coastal sea level to monitor eastern Pacific equatorial Kelvin waves. *J. Phys. Oceanogr.,* **22,** 163–183.

——, and C. Shi, 1991: Critical frequencies at ocean boundaries. *J. Geophys. Res.,* **96,** 10 731–10 738.

——, and X. Liu, 1994: Interannual sea level in the northern and eastern Indian Ocean. *J. Phys. Oceanogr.,* **24,** 1224–1235.

——, and S. Van Gorder, 1994: On ENSO coastal currents and sea levels. *J. Phys. Oceanogr.,* **24,** 661–680.

——, and J. Li, 2004: El Niño/La Niña shelf edge flow and Australian western rock lobsters. *Geophys. Res. Lett.,* **31,** L11301, doi: 10.1029/2003GL018900.

Ebisuzaki, W., 1997: A method to estimate the statistical significance of a correlation when the data are serially correlated. *J. Climate,* **10,** 2147–2153.

Grimshaw, R., and J. S. Allen, 1988: Low-frequency baroclinic waves off coastal boundaries. *J. Phys. Oceanogr.,* **18,** 1124–1143.

Killworth, P. D., D. B. Chelton, and R. A. Szoeke, 1997: The speed of observed and theoretical long extratropical planetary waves. *J. Phys. Oceanogr.,* **27,** 1946–1966.

Lenanton, R. C., L. Joll, J. Penn, and K. Jones, 1991: The influence of the Leeuwin Current on coastal fisheries of western Australia. *J. Roy. Soc. W. Aust.,* **74,** 101–114.

MacCready, P., and P. B. Rhines, 1993: Slippery bottom boundary layers on a slope. *J. Phys. Oceanogr.,* **23,** 5–22.

Pariwono, J. I., J. A. T. Bye, and G. W. Lermon, 1986: Long-period variations of sea level in Australia. *Geophys. J. Roy. Astron. Soc.,* **87,** 43–54.

Pizarro, O., A. J. Clarke, and S. Van Gorder, 2001: El Niño sea level and currents along the South American coast: Comparison of observation with theory. *J. Phys. Oceanogr.,* **31,** 1891–1903.

Schopf, P. S., D. L. T. Anderson, and R. Smith, 1981: Beta-dispersion of low-frequency Rossby waves. *Dyn. Atmos. Oceans,* **5,** 187–214.

Tomczak, M., and J. S. Godfrey, 1994: *Regional Oceanography: An Introduction.* Pergamon, 422 pp.

Trenberth, K. E., 1984: Signal versus noise in the Southern Oscillation. *Mon. Wea. Rev.,* **112,** 326–332.

Trowbridge, J. H., and S. J. Lentz, 1991: Asymmetric behavior of an oceanic boundary layer above a sloping bottom. *J. Phys. Oceanogr.,* **21,** 1171–1185.